Acta Crystallographica Section D
Biological Crystallography
ISSN 0907-4449

Structure of a complete four-domain chitinase from *Moritella marina*, a marine psychrophilic bacterium

Piotr H. Malecki,[a] Joanna E. Raczynska,[a]‡ Constantinos E. Vorgias[b] and Wojciech Rypniewski[a]*

[a]Institute of Bioorganic Chemistry, Polish Academy of Sciences, Noskowskiego 12/14, 61-704 Poznan, Poland, and [b]Department of Biochemistry and Molecular Biology, National and Kapodistrian University of Athens, Zografou Campus, 15701 Athens, Greece

‡ Present address: UT Southwestern Medical Center, 5323 Harry Hines Boulevard, Dallas, TX 75390-8816, USA

Correspondence e-mail: wojtekr@ibch.poznan.pl

Received 30 October 2012
Accepted 21 January 2013

PDB References: *Mm*Chi60, 4hmc; complex with NAG_4, 4hmd; complex with NAG_3, 4hme

X-ray crystallography reveals chitinase from the psychrophilic bacterium *Moritella marina* to be an elongated molecule which in addition to the catalytic β/α-barrel domain contains two Ig-like domains and a chitin-binding domain, all linked in a chain. A ligand-binding study using NAG oligomers showed the enzyme to be active in the crystal lattice and resulted in complexes of the protein with oxazolinium ion (the reaction intermediate) and with NAG_2, a reaction product. The characteristic motif D*X*D*X*E, containing three acidic amino-acid residues, which is a signature of type 18 chitinases, is conserved in the enzyme. Further analysis of the unliganded enzyme with the two protein–ligand complexes and a comparison with other known chitinases elucidated the roles of other conserved residues near the active site. Several features have been identified that are probably important for the reaction mechanism, substrate binding and the efficiency of the enzyme at low temperatures. The chitin-binding domain and the tryptophan patch on the catalytic domain provide general affinity for chitin, in addition to the affinity of the binding site; the two Ig-like domains give the protein a long reach over the chitin surface, and the flexible region between the chitin-binding domain and the adjacent Ig-like domain suggests an ability of the enzyme to probe the surface of the substrate, while the open shallow substrate-binding groove allows easy access to the active site.

1. Introduction

A wide variety of microorganisms are present in cold environments, displaying a diverse range of adaptations. The major part of the marine biosphere is characterized by permanent low temperatures (271–283 K) and therefore is a good source of cold-adapted marine bacteria, the so-called psychrophilic bacteria. Chitin is a very abundant insoluble biopolymer in the marine environment and is composed of linear chains of β-1,4-linked *N*-acetyl-D-glucosamine residues, with the chains closely connected by hydrogen bonds. After cellulose, chitin is the second most abundant biopolymer in nature. It is a crucial structural component of the cell walls of fungi and certain green algae and is a major constituent of the shells, cuticles and exoskeletons of worms, molluscs and arthropods, including crustaceans and insects (Muzzarelli, 1977). Chitin and its partially deacetylated derivative chitosan, as well as other derivatives, exhibit interesting properties and constitute a valuable raw material for biomedical, agricultural, cosmetics and innovative biotechnological applications (Shigemasa & Minami, 1996). In the aquatic biosphere, approximately 10^{11} tons of chitin are produced annually (Keyhani & Roseman, 1999).

Chitinases (EC 3.2.1.14) hydrolyse the β-1,4-linkages in chitin. The currently sequenced or identified chitinases have been classified into two families, 18 and 19, within the glycosyl hydrolase superfamily established by Henrissat and Bairoch based on the amino-acid sequence similarity of their catalytic regions (Henrissat & Bairoch, 1993). Family 18 contains chitinases from bacteria, fungi, viruses and animals, and some plant chitinases. Family 19 contains plant chitinases and a few bacterial chitinases, such as *Streptomyces griseus* chitinase C (Ohno *et al.*, 1996). Chitinases of the two families do not share amino-acid sequence similarity and have different three-dimensional structures (Perrakis *et al.*, 1994; Terwisscha van Scheltinga *et al.*, 1996) and enzymatic mechanisms, and are therefore believed to have evolved from diverse ancestors. Bacterial chitinases generally consist of multiple functional domains such as chitin-binding domains (classed among the carbohydrate-binding modules; CBMs) and fibronectin type III-like domains (Fn3 domain) linked to the catalytic domain. The involvement of chitin-binding modules in the degradation of insoluble chitin has been analysed for a few bacterial chitinases (Svitil & Kirchman, 1998; Watanabe *et al.*, 1994).

Chitinases produced by psychrophilic bacteria, which are responsible for degradation of krill chitin, should have high catalytic activities under these low-temperature conditions and most often, if not always, exhibit high thermosensitivity (Gerday *et al.*, 1997). These properties can be very useful for various applications. In the past few years, several psychrophilic enzymes have been discovered (Luo *et al.*, 2006; Yaish *et al.*, 2006) and the primary structures of some have been determined (Aghajari *et al.*, 2003; Van Petegem *et al.*, 2003; Violot *et al.*, 2005). Until recently, few psychrophilic chitinases had been isolated from bacteria (Bendt *et al.*, 2001; Lonhienne *et al.*, 2001; Orikoshi *et al.*, 2003) and fungi (Fenice *et al.*, 1998); however, only the catalytic domain of one other psychrophilic chitinase, from *Arthrobacter* TAD20, has been solved (M. Ayati, D. Mandelman, N. Aghajari & R. Haser, unpublished work; PDB entry 1kfw).

In this work, we report the crystal structure of a chitinase from the psychrophilic bacterium *Moritella marina*. This four-domain enzyme is the most complex crystallographic structure of a glycoside hydrolase solved to date. The enzyme has been examined in complexes with the reaction intermediate and with the reaction product and in an unliganded form.

2. Methods

2.1. Bacterial strains, plasmids, DNA manipulations and other materials

The bacterial strain *M. marina* (synonym *Vibrio marinus*; ATCC 15381) isolated from a sample raised from a depth of 1200 m and a temperature of 276.3 K in the Northern Pacific Ocean was the initial source of our biological material (Morita & Haight, 1964). The bacterial cells were grown at the temperature of 288 K for 48 h in Bacto Marine broth medium 2216 (Difco, USA).

2.2. Overproduction and purification of *Mm*Chi60 protein

The chitinase gene named *Mm*Chi60 from *M. marina* was cloned as described in Stefanidi & Vorgias (2008). Briefly, the *Mm*Chi60 gene was further cloned into the T7 expression vector pET-11a by ligating the *Nde*I–*Bam*HI fragment of the clone pCR2.1-*Mm*Chi60 to *Nde*I–*Bam*HI-digested pET-11a vector. Ligated plasmids were used to transform *Escherichia coli* BLR (DE3) host cells. Induction of host cells harbouring the pET-11a-*Mm*Chi60 plasmid was performed in Luria–Bertani (LB) medium containing 100 μg ml^{-1} ampicillin at 310 K. The culture was induced with 0.5 m*M* isopropyl β-D-1-thiogalactopyranoside (IPTG) at the mid-exponential growth phase and was further incubated at 291 K. Samples were withdrawn at various time points. For large-scale production the induction time was 3 h. The produced bacterial cells in 3.5 g quantities were either used immediately or kept frozen until needed. All extraction and purification procedures were performed at 277 K, except where specified otherwise. Cells were harvested by centrifugation at 8000*g*, washed and suspended (10 ml g^{-1}) in 20 m*M* sodium phosphate buffer pH 8.0, 100 m*M* NaCl, 1 m*M* EDTA, 0.5%(*v*/*v*) Triton X-100, 0.5 m*M* phenylmethanesulfonyl fluoride (PMSF). The cells were disrupted by sonication and the lysate was centrifuged at 12 000*g* for 1 h. The clear supernatant was further fractionated with solid ammonium sulfate. *Mm*Chi60 activity was detected in the fraction of 40–60% saturation with ammonium sulfate. This protein fraction was dissolved in 20 m*M* sodium phosphate buffer pH 8.0, 0.5 *M* ammonium sulfate and directly applied onto a 10 ml Phenyl-Sepharose CL-6B column (Pharmacia, Sweden) previously equilibrated in the same buffer. The column was washed with the same buffer and bound proteins were eluted with a 100 ml descending gradient of 0.5–0 *M* ammonium sulfate. *Mm*Chi60 eluted at approximately 0.1 *M* ammonium sulfate. The pooled *Mm*Chi60 fractions were diluted fivefold with 20 m*M* sodium phosphate buffer pH 8.0 and directly applied onto a 10 ml Q-Sepharose Fast Flow column (Pharmacia) previously equilibrated in the same buffer. Bound proteins were eluted using a 100 ml linear ascending gradient of 0–0.5 *M* NaCl. Pure *Mm*Chi60 was eluted at approximately 0.45 *M* NaCl. Enzymatically active and pure *Mm*Chi60 fractions were pooled and stored at 277 K. The purified enzyme was stable for at least three months under these conditions. Gel-filtration column chromatography of pure *Mm*Chi60 was performed using a Superdex 200 column (1.6 $\times$ 60 cm, Pharmacia) in 20 m*M* Tris buffer, 500 m*M* NaCl pH 7.0. The N-terminal 22-residue signal peptide was present in the cloned gene sequence but was absent in the purified enzyme. This was confirmed by mass spectrometry. Apparently, the *E. coli* cell secretion apparatus recognized and processed the signal peptide of the chitinase.

2.3. Crystallization and X-ray data collection

All *Mm*Chi60 crystals were grown using the hanging-drop vapour-diffusion method at 277 K. The well solution consisted of 23%(*w*/*v*) PEG 4000, 0.16 *M* ammonium sulfate, 0.1 *M* citrate buffer pH 5.5. The protein solution consisted of

3 mg ml^{-1} *Mm*Chi60, 0.02 *M* Tris buffer pH 7.0, 0.5 *M* NaCl. Crystallization drops were prepared by mixing the protein solution with the well solution in a 2:1 or a 3:1 ratio. Protein crystals appeared after approximately two weeks. The NAG ligands were soaked in by adding the ligand to the cryosolution at a concentration exceeding the protein concentration by approximately 5:1. Soaking experiments were performed with *N*,*N*′,*N*″-triacetyl chitotriose (NAG_3) and with *N*,*N*′,*N*″,*N*‴-tetra-acetyl chitotetraose (NAG_4). The cryosolution contained 25%(*v*/*v*) glycerol in a solution similar to the well solution. The crystals were immersed in the cryosolution for approximately 30 s prior to freezing at 100 K in the cryostream. The crystal used in the SAD measurement was soaked for 20 min in cryosolution to which KBr had been added to a concentration of 0.5 *M*. All soaking experiments were performed at 277 K, which is close to the living temperature of *M. marina*, and care was generally taken to maintain the *Mm*Chi60 crystals at cold-room temperature until the moment of freezing. X-ray diffraction data were collected on beamline 14.2 at the BESSY synchrotron in Berlin using a MAR Research MX-225 detector. The data were integrated and scaled using the *HKL*-2000 software (Otwinowski & Minor, 1997) and *XDS* (Kabsch, 2010). A summary of the X-ray data statistics is given in Table 1.

Table 1
Summary of X-ray data collection and refinement.

Values in parentheses are for the highest resolution shell.

	*Mm*Chi60	*Mm*Chi60–NAG_3	*Mm*Chi60–NAG_4	*Mm*Chi60–Br
PDB code	4hmc	4hme	4hmd	—
Space group	$P3_112$	$P3_112$	$P3_112$	$P3_112$
Unit-cell parameters				
$a = b$ (Å)	67.62	66.00	67.09	67.81
c (Å)	257.19	257.54	258.03	259.68
Beamline	BESSY BL14.2	BESSY BL14.2	BESSY BL14.2	BESSY BL14.2
Wavelength (Å)	0.91841	0.91841	0.91841	0.92001
Resolution (Å)	50.0–2.10 (2.14–2.10)	50.0–2.07 (2.11–2.07)	50.0–2.26 (2.32–2.26)	50.0–2.70 (2.75–2.70)
R_{merge}†	0.071 (0.451)	0.114 (0.940)	0.098 (0.979)	0.134 (0.869)
Completeness (%)	95.5 (70.0)	99.5 (99.1)	99.3 (98.0)	100.0 (100.0)
Observed reflections	323034	359867	292099	154117
Unique reflections	39878	39522	31416	19182
$\langle I/\sigma(I)\rangle$	28.1 (2.3)	20 (1.9)	21.1 (2.4)	14.4 (1.8)
Multiplicity	8.5	9.1	7.5	8.0
R‡	0.19	0.18	0.19	
R_{free}§	0.24	0.21	0.25	
Protein atoms	4137	4137	4137	
Ligand atoms	7	54	35	
Water molecules	261	292	167	
Average B factor (Å^2)	44	51	47	
Error in Luzzati plot (Å)	0.20	0.17	0.25	
R.m.s. deviation from ideal				
Bond lengths (Å)	0.018	0.020	0.016	
Bond angles (°)	1.87	1.85	1.76	
Ramachandran plot (%)				
Most favoured	96.2	97.9	96.0	
Additionally allowed	3.6	1.9	3.8	
Disallowed	0.2	0.2	0.2	

† $R_{merge} = \sum_{hkl}\sum_i |I_i(hkl) - \langle I(hkl)\rangle| / \sum_{hkl}\sum_i I_i(hkl)$, where $I_i(hkl)$ is the integrated intensity of a given reflection and $\langle I(hkl)\rangle$ is the mean intensity of multiple corresponding symmetry-related reflections. ‡ $R = \sum_{hkl} ||F_{obs}| - |F_{calc}|| / \sum_{hkl} |F_{obs}|$, where F_{obs} and F_{calc} are the observed and calculated structure factors, respectively. § R_{free} is R calculated using a randomly chosen 1000 reflections that were excluded from the refinement.

2.4. Structure determination and refinement

The phase problem was solved for *Mm*Chi60 by the MR-SAD method as implemented in the *Auto-Rickshaw* pipeline (Panjikar *et al.*, 2005) using the *Mm*Chi60–Br data (Table 1). Briefly, a partial molecular-replacement (MR) solution was obtained with *MOLREP* (Vagin & Teplyakov, 2010) using the crystal structure of chitinase from *Lactococcus lactis* (New York SGX Research Center for Structural Genomics, unpublished work; PDB entry 3ian) stripped of solvent molecules as the search model. The MR model at this stage, consisting of a TIM β/α-barrel, included 309 amino-acid residues and corresponded to approximately 60% of the *Mm*Chi60 structure. The MR model was pre-refined with *REFMAC*5 (Murshudov *et al.*, 2011) and was used in a maximum-likelihood SAD phasing calculation with *Phaser* (McCoy *et al.*, 2007) to improve the phases and to identify the sites of Br anomalous scatterers. The positions and occupancy factors of the heavy atoms were refined with *MLPHARE* (Winn *et al.*, 2011), *SHARP* (Bricogne *et al.*, 2003) and *BP*3 (Pannu & Read, 2004). The resulting phases were improved using *Pirate* by applying real-space constraints based on known features of a protein electron-density map (Cowtan, 2000). Next, a polyalanine model of as yet uninterpreted regions of electron density was constructed using *SHELXE* (Sheldrick, 2008). Following this, a round of automatic model building was performed using *RESOLVE* (Terwilliger, 2003) and *Buccaneer* (Cowtan, 2008). The updated model was refined with *REFMAC*5 (Murshudov *et al.*, 2011). A total of six cycles of phasing, heavy-atom search and model building were performed as described above. In the end, 12 bromide sites were identified in the anomalous map above the 3σ level. Three of the peaks were greater than 10σ. The R factor and R_{free} for the atomic model at this stage were 0.31 and 0.38, respectively. The final model was obtained after cycles of manual adjustments using *Coot* (Emsley *et al.*, 2010) and *REFMAC*5 (Murshudov *et al.*, 2011). The other *Mm*Chi60 structures were solved by MR using the model obtained as described above. In addition to *REFMAC*5, *PHENIX* was used for model refinement (Afonine *et al.*, 2012).

2.5. Sequence comparison

Internal sequence alignment was carried out using *LALIGN* (Huang & Miller, 1991). The *BLAST* algorithm was used to find the most relevant sequences (Altschul *et al.*, 1990).

3. Results

3.1. The overall structure

The final models are summarized in Table 1. In the crystal lattice the *Mm*Chi60 molecules are nested pairwise against each other around the twofold axes (Fig. 1). The *Mm*Chi60 molecule consists of 528 amino-acid residues (23–550) arranged in four domains: the N-terminal catalytic β/α-barrel domain (residues 23–342; classed as glycoside hydrolase family 18; GH18), two bacterial immunoglobulin-like (Ig-like) domains known as Big 3 domains (Pfam database ID PF07523; residues 348–421 and 422–501) and the C-terminal chitin-binding domain (residues 507–550). The fold of the chitin-binding domain is recognized as a carbohydrate-binding module of type A (Boraston *et al.*, 2004) family 5 (Akagi *et al.*, 2006), abbreviated as CBM5, with some specific chitin-binding features (see below). The domains are arranged linearly, giving the molecule an elongated sea-horse shape (Fig. 2). The electron density of the main chain is continuous except at Val505 between the chitin-binding domain and the adjacent Ig-like domain. The two cysteine residues present in the sequence (Cys41 and Cys53) form a disulfide bridge at the base of the hairpin formed by β-strands 43–44 and 50–51. A sodium-binding site was identified in the catalytic domain. The cation is coordinated by the side chains of Asn105 and Asp146, the carbonyl O atom of Gly144, the carbonyl O atom of Thr24 (2.6–2.7 Å) and a water molecule (2.2–2.4 Å). A

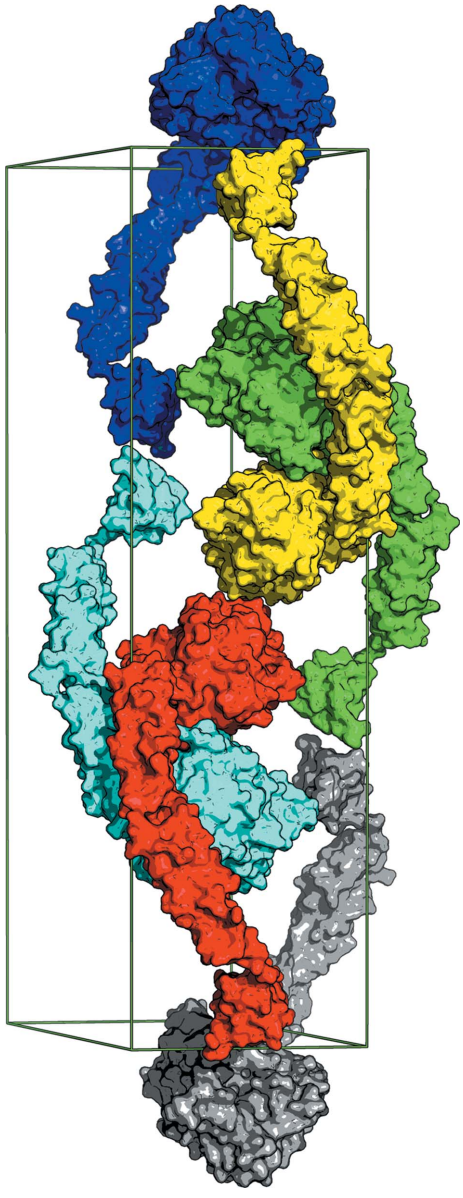

Figure 1
Crystal packing. Surface representation of *Mm*Chi60 molecules in the unit cell. The molecules pack pairwise around the crystal twofold axes. This and the other figures were prepared with *PyMOL* (DeLano, 2002).

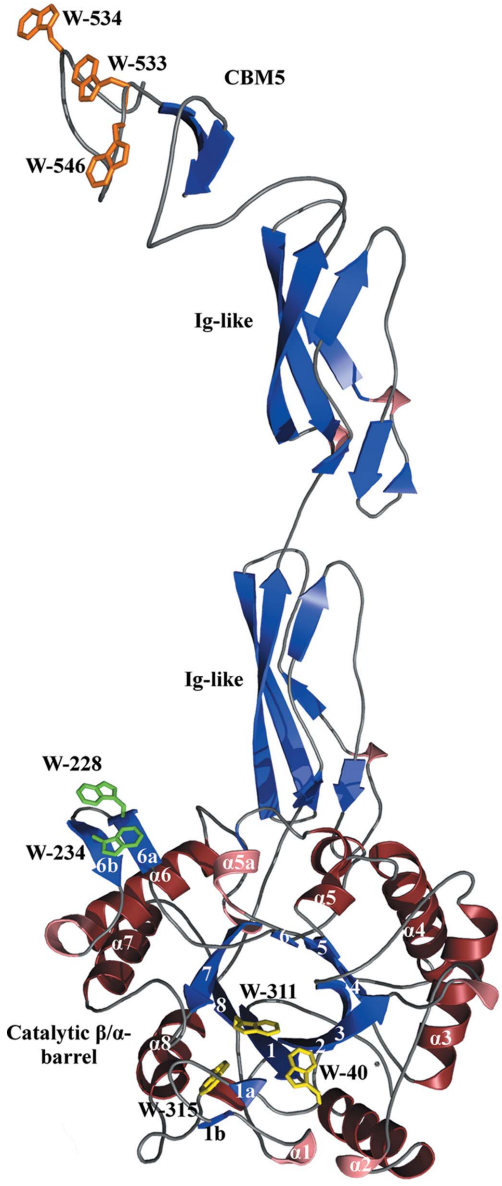

Figure 2
Cartoon plot of *Mm*Chi60. The four protein domains are labelled. The secondary-structure elements (α-helices, red; β-sheets, blue; 3_{10}-helices, pink) of the catalytic domain are labelled according to the convention for β/α-barrels. Tryptophan residues believed to be significant in chitin binding are shown and labelled: Trp residues in the chitin-binding domain, orange; the Trp patch on the catalytic domain, green; Trp residues lining the active site, yellow.

sodium site was found in a corresponding position in the chitinase from *L. lactis* (New York SGX Research Center for Structural Genomics, unpublished work; PDB entry 3ian). The linker between the catalytic domain and the first Ig-like domain begins with a pair of proline residues (Pro343 and Pro344). The linker is well ordered and contacts the β/α-barrel *via* buried water molecules and polar side chains on the surface of the catalytic domain. Each Ig-like domain is a bundle of five β-strands (with the third strand being interrupted by a 3_{10}-helix). The β-strands are antiparallel except for the first and the last, which are parallel (a consequence of the odd number of strands in the bundle). The two Ig-like Big 3 domains show 40% identity (75% similarity) between their core regions of 77 amino acids. There is no clear pattern to the conservation. According to the Pfam server (Finn *et al.*, 2010) Big 3 domains are found in cell-wall adhesion proteins and in various glycoside hydrolases.

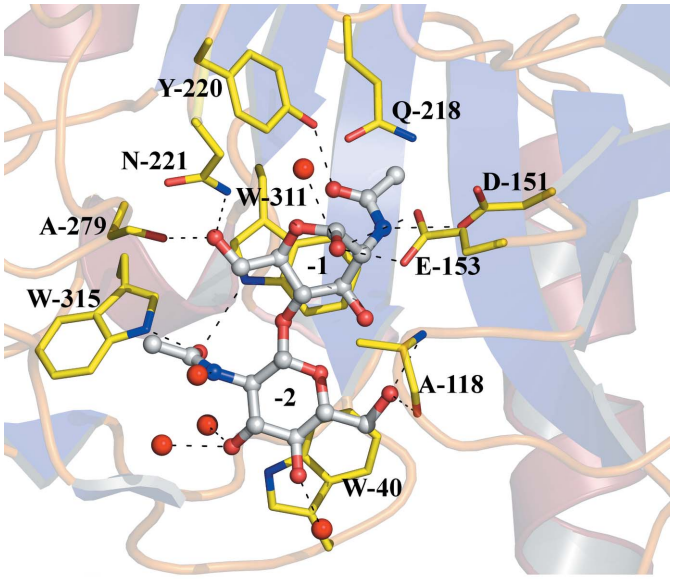

(*a*)

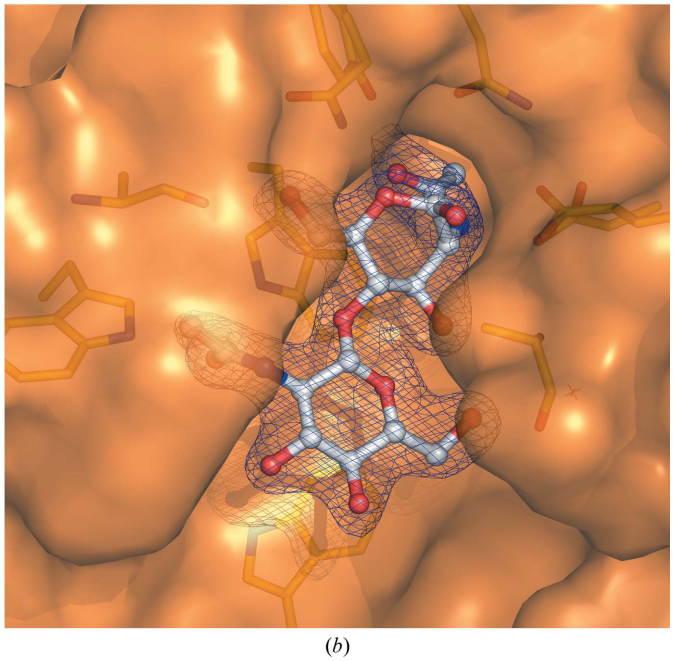

(*b*)

Figure 3
(*a*) Details of the interaction between the reaction product NAG_2 and *Mm*Chi60. Hydrogen bonds between the ligand and the binding site of the protein and water molecules (red spheres) are indicated as dashed lines. (*b*) Surface representation showing the ligand-binding cavity and a weighted $2F_o - F_c$ map contoured around the ligand at the 2σ level.

3.2. Chitin binding

The small 44-residue chitin-binding (CMB5) domain contains six Trp residues, of which three contribute to the hydrophobic core (Trp510, Trp529 and Trp549); the other three (Trp533, Trp534 and Trp546) are exposed on the surface and their side chains are coplanar (Fig. 2). Two of the exposed Trp residues are conserved in other known chitin-binding domains of the same class CBM5: ChiC from *S. griceus* (Akagi *et al.*, 2006) and ChiB from *Serratia marcescens* (van Aalten *et al.*, 2000). The third, Trp546, has not been observed in other crystal structures. It resides on a three-residue insertion that forms a small loop. The distance between the exposed Trp side chains in *Mm*Chi60 is 10–11 Å, which corresponds to the length of two NAG units, *i.e.* the period of the poly-NAG chain in chitin.

A similar surface feature consisting of two nearly coplanar Trp residues (Trp228 and Trp234) is found on the catalytic domain (Fig. 2). The distance between the two exposed side chains is 7.3 Å. A similar feature is found in the chitinase from *L. lactis* (PDB entry 3ian) and in ChiC from *S. marcescens* (Payne *et al.*, 2012). No NAG ligands were found to be associated with the two surface Trp clusters in the crystal lattice.

3.3. Substrate-binding groove

The substrate-binding groove is located at the carboxyl ends of the β-strands of the β/α-barrel, similar to other enzymes with a TIM-barrel architecture. In the unliganded *Mm*Chi60

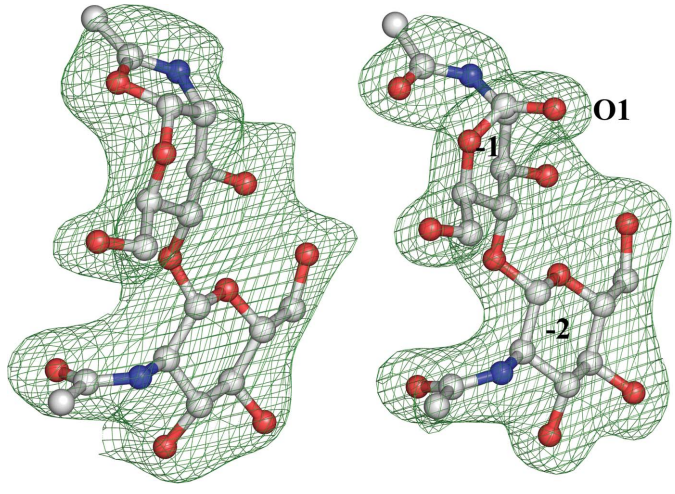

Figure 4
Comparison of the omit $F_o - F_c$ maps, contoured at the 3σ level, of ligands found in the binding groove of *Mm*Chi60. The reaction intermediate (an oxazolinium ion) in the −1 subsite (left) and the reaction product (an NAG moiety) featuring the electron density of the O2 atom (right). The −2 subsite is occupied by an NAG residue in both complexes.

structure the groove is only occupied by solvent water molecules. In the structure soaked in NAG_3, an NAG_2 ligand was observed in the substrate-binding subsites −1 and −2 (Davies *et al.*, 1997; Fig. 3). In the structure soaked in NAG_4, a ligand of similar size to NAG_2 but with distinct features was observed in the −1 site. There was no electron density for the O1 atom, and the density of the *N*-acetyl chain indicated the formation of an oxazolinium ring. Subsequently, the ligand density was interpreted as an oxazolinium-ion reaction intermediate (Fig. 4). The differences in the ligand structure are accompanied by local differences in the protein structure and the solvent (see below).

The bottom of the substrate-binding groove is lined by Trp40, Trp311 and Trp315 (Fig. 2). The first two Trp residues make stacking interactions with the two NAG moieties in the substrate-binding site. In addition to the stacking, Trp311 forms a hydrogen bond to the carbonyl O atom of the *N*-acetyl group of the NAG unit in the −2 site. The side chain of Trp315 provides another hydrogen bond to the same O atom (Fig. 3*a*).

The substrate-binding groove in *Mm*Chi60 is relatively shallow (Fig. 3*b*) compared with the other well known chitinase structures, *e.g.* ChiA (Perrakis *et al.*, 1994; PDB entry 1ctn) and ChiB (van Aalten *et al.*, 2000; PDB entry 1e15) from *S. marcescens*, which both have additional loops on both sides of the substrate-binding groove and an $\alpha+\beta$ domain inserted in the TIM barrel on the 'plus' side of the substrate-binding site. Among the known structures, the substrate-binding groove in *Mm*Chi60 is most similar to those of the chitinase from *L. lactis* (PDB entry 3ian), ChiC from *S. marcescens* (Payne *et al.*, 2012) and the chitinase from *Bacillus cereus* (Hsieh *et al.*, 2010).

3.4. The active site

The active site lies at the bottom of the substrate-binding cleft, at the junction between the −1 and +1 subsites, where the cleft bends sharply. The curvature of the binding groove is similar to other chitinases and has been shown to induce bending of the poly-NAG chain at the scissile β-1,4-glycosidic bond, forcing the sugar ring in the −1 site into the boat conformation (Papanikolau *et al.*, 2001). In the complex of *Mm*Chi60 with the NAG_2 reaction product the sugar ring is indeed found in the boat conformation. In the complex with the oxazolinium-ion reaction intermediate the sugar ring is in the chair conformation. A cavity at the bottom of the −1/+1 junction is directed into the body of the protein down the axis of the β/α-barrel, and accommodates the *N*-acetyl group of the '−1' NAG unit or contains the oxazolinium ring of the bound reaction intermediate.

The active site contains two conserved acidic side chains, Asp151 and Glu153, which are part of the D*X*D*X*E signature of glycosyl hydrolases belonging to family 18 (Henrissat & Davies, 1997). The conformation of Asp151 is unchanged in the three *Mm*Chi60 structures, but Glu153 changes its position relative to Asp151. In the complex of *Mm*Chi60 with NAG_2 the distance between the neighbouring carboxyl O atoms of Asp151 and Glu153 is 3.1 Å, indicating the presence of an H atom between them. In the ligand-free structure and in the complex with the oxazolinium-ion reaction intermediate the corresponding distance between the two residues is approximately 10 Å. This is owing to a shift in the main chain and a flip of the Glu153 side chain. The flipping of the side chain results in a distortion from planarity of the peptide bond between residues 152 and 153, which is reflected in the value of the ω torsion angle (160°). The space vacated by the displaced side chain is occupied by electron density which can accommodate a water molecule and has been modelled thus. The flipping of the Glu153 side chain is accompanied by a shift of residues Gly117–Ile122 and a rotation of the main chain of Ala120-His121. In effect, the carbonyl O atom of Ala120 moves by approximately 5 Å and its place is taken by the carboxyl group of Glu153, the O atoms of which form hydrogen bonds to Asp119 N (2.8 Å) and Ala120 N (2.9 Å) (Fig. 5).

A close contact exists between the C1 atom of the oxazolinium intermediate and the carbonyl O atom of the Gln218 side chain (3.1 Å), indicating a C—H···O hydrogen bond. The distance from the carbonyl O atom to the O atom of the oxazolinium ring is 2.8 Å: a close Van der Waals contact (see §4).

Some residual difference electron density in the structure at and around the oxazolinium ion indicates a low-occupancy species similar to the structure with the NAG_2 reaction product. However, the occupancy was too low for meaningful modelling.

The O6 hydroxyl of NAG in the −1 subsite is bound to the $N^{\delta2}$ amine group of Asn221 and the carbonyl O atom of Ala279 (Fig. 3*a*). This is a different coordination of the O6 hydroxyl from that found in the chitinases ChiA and ChiB from *S. marces-*

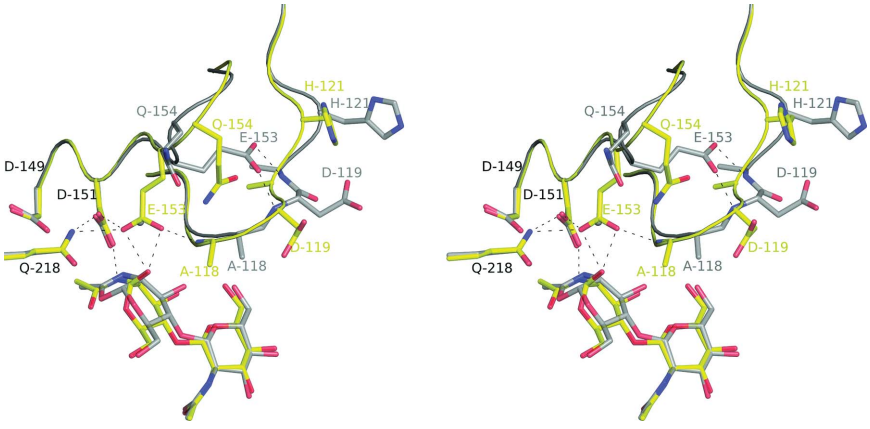

Figure 5
Stereo pair showing a comparison of *Mm*Chi60 structures with the bound oxazolinium reaction intermediate (grey sticks and labels) and with the NAG_2 reaction product (yellow sticks and labels). Black labels are used for structurally unchanged residues. The different stages of ligand processing are accompanied by significant rearrangements of residues in the binding site, especially the active residue Glu153 and the flexible loop 117–122. Black dashes indicate the hydrogen bonds of Asp151, Glu153 and other residues.

cens, which have an Asp in the place of Asn221 (a hydrogen-bond acceptor instead of a donor) and in which the O6 hydroxyl does not make a hydrogen bond to the main chain. The arrangement found in the present structures is similar to that found in the chitinase from *B. cereus* (Hsieh *et al.*, 2010; PDB entry 3n11) and a plant chitinase/lysozyme (hevamine) from *Hevea brasiliensis* (Terwisscha van Scheltinga *et al.*, 1996; PDB entry 1llo).

4. Discussion

4.1. What is the place of *Mm*Chi60 among other chitinases?

The common feature of family 18 chitinases is the β/α-barrel fold of the catalytic domain and the conserved sequence motif D*X*D*X*E. However, *Mm*Chi60 shows clear amino-acid sequence similarity to only two other chitinases for which the structure has been determined experimentally: the chitinase from *L. lactis* (57% identity within the catalytic domain; PDB entry 3ian) and ChiC from *S. Marcescens* (56% identity; Payne *et al.*, 2012). The next most similar are the chitinase from *B. cereus* (29%) and the plant chitinase hevamine (23%). The catalytic domains of the four enzymes appear to be similar to the catalytic domain of *Mm*Chi60 in that they all form shallow substrate-binding grooves, as opposed to ChiA and ChiB from *S. marcescens*, which have insertions in the basic topology of the β/α-barrel that make the binding sites deeper or 'tunnel-like'. The deep binding grooves of these enzymes have been attributed to their processivity (Zakariassen *et al.*, 2009). In *Mm*Chi60, the shallow substrate-binding groove has fewer aromatic residues, especially on the '+' (aglycon) side. One feature that *Mm*Chi60 shares with ChiA, which is absent in ChiB, is the presence of Trp40 in the −3 subsite. The corresponding residue in ChiA (Trp167) was shown to sustain its processivity toward chitin, while its substitution by Ala increased the hydrolytic activity of the enzyme towards chitosan (a partially deacetylated water-soluble chitin derivative). The issue of the processivity of *Mm*Chi60 has not been investigated. However, it can be noted that according to recently published work a shallow binding groove and flexible elements in the enzymatic machinery suggest a nonprocessive working mode (Payne *et al.*, 2012).

A remarkable similarity exists between *Mm*Chi60 and chitinase A1 from *B. circulans* (Toratani *et al.*, 2006). Studies of the latter by a combination of techniques revealed a similar arrangement of domains to *Mm*Chi60. Chitinase A1 has the catalytic β/α-barrel at one end and the chitin-binding domain at the other end, and a tandem of two fibronectin type III (FnIII) domains corresponding to the tandem of bacterial Ig-like (Big 3) domains in *Mm*Chi60. The two types of domain are superficially similar except that the Big 3 domains have only five β-strands each, lacking the two 'meandering' strands of the Greek-key motif. The two Big 3 domains of *Mm*Chi60 are the first X-ray structures of this type of domain. One structure of such a domain has been determined by NMR (Northeast Structural Genomics Consortium, unpublished work; PDB entry 2kpn).

4.2. What is the biological significance of the observed crystal structures of *Mm*Chi60?

Analysis of the complexes shows that the enzyme is active in the crystal form. Enzymatic activity of crystallized enzymes has been noted many times previously. In a previously reported experiment with another bacterial chitinase, the protein crystal was soaked in NAG_4 for 24 h and only a single sugar ring was found in the binding site of the enzyme (Perrakis *et al.*, 1994). In the present study NAG_3 has been reduced to NAG_2, which appears to be a stable product of this enzyme. In the soaking experiment with NAG_4 the oxazolinium reaction intermediate has been captured in the crystal. This is fortunate but not completely unexpected. The soaking times were deliberately short (only as long as it took to cryoprotect the crystal) in the hope of capturing interesting protein–ligand complexes. Trapping reaction intermediates is usually difficult and requires special measures or conditions to slow the reaction, as demonstrated for *O*-GlcNAc hydrolase (He *et al.*, 2010). This was not the case here and the pH of 5.5 was close to optimal for the enzymatic reaction (Stefanidi & Vorgias, 2008). We suspect that the observation of the reaction intermediate is in this case strongly dependent on the time of soaking and the initial concentration of the substrate.

4.3. What do we learn about the reaction mechanism?

Comparison of the three *Mm*Chi60 structures with those of other previously reported chitinases can be used to identify structural features relevant to the catalytic mechanism. Firstly, the D*X*D*X*E signature of family 18 chitinases is conserved (it corresponds to Asp149-Ile150-Asp151-Leu152-Glu153) and the *Mm*Chi60 structures provide new information about its position and conformational changes at different points along the course of the enzymatic reaction. The most mobile residue in this study is Glu153, which is considered to be the acid/base in the reaction mechanism. In *Mm*Chi60, this residue flips between two positions more than 7 Å apart. In the unliganded structure it points away from the active site and its carboxyl group is apparently 'parked' stably against two main-chain NH groups of a flexible loop that positions itself accordingly, while a water molecule occupies its place in the active site. The structure obtained in the absence of ligands can be considered to be the resting state of the enzyme. A similar arrangement is observed in the complex with the reaction intermediate. In this structure we see one of the elements necessary for hydrolysis of the oxazolinium intermediate, a water molecule, but the base is distant. In the complex with NAG_2 hydrolysis has already taken place. The active Glu has moved in and the water molecule is no longer present, but a hydroxyl group has been added to the sugar ring (Fig. 4). A similar remote position of an equivalent Glu was discovered in the chitinase from *L. lactis*, but was not discussed. Recently, it was described in ChiC from *S. marcescens* (Payne *et al.*, 2012). In the chitinase from *B. cereus* a corresponding flexible loop was described, but without flipping of the catalytic Glu (Hsieh *et al.*, 2010). The flipping of the catalytic Glu153 and the shifting of the adjacent residues in the presence of the reaction product can

be compared with the ligand-induced conformational change described for other types of glycoside hydrolases (Varrot *et al.*, 2000).

Asp151 is the middle of the three conserved residues of the chitinase D*X*D*X*E signature. In earlier studies this residue was proposed to rotate between the other two acidic side chains, shuttling a proton to the active site. It was reported to be in the 'down' position in the unliganded (resting) state of ChiB (van Aalten *et al.*, 2001) and in two alternative, 'up' or 'down', orientations in unliganded ChiA (Papanikolau *et al.*, 2003). The switching observed in ChiA and ChiB from *S. marcescens* was accompanied by adjusting movements of the neighbouring Ser and Tyr residues. This Ser was examined and was discovered to be important for the catalytic mechanism; its mutation to Ala reduced the specific activity 20-fold (Synstad *et al.*, 2004). A comparison of *Mm*Chi60 with other chitinases reveals different conformations of the key residues and amino-acid substitutions around them. Firstly, Asp151 points away from Asp149 in all three *Mm*Chi60 structures, including the unliganded enzyme. No contact is observed between the two residues. Secondly, the aforementioned Ser, the mutation of which to Ala was debilitating to ChiB, occurs naturally in *Mm*Chi60 (Ala114). The 'up' position of Asp151 is stabilized by three hydrogen bonds: (i) to the NH group of the *N*-acetyl moiety of the ligand in the active site, (ii) to the catalytic Glu153, when it is directed toward the active site (3.1 Å in the complex with NAG_2), indicating a proton in between and (iii) to the NH_2 group of Gln218 (3.3 Å) (Fig. 5). Interactions (i) and (ii) have been described in the previously proposed reaction mechanism (van Aalten *et al.*, 2001), but the third hydrogen bond is not observed in most chitinase structures because they have Met instead of Gln. The residue in this position is interesting because of its interaction with the ligand in the active site. In *Mm*Chi60, the carbonyl O atom of Gln218 is in close contact with the O atom of the oxazolinium ring of the reaction intermediate (3.1 Å). It is also close to C1 (3.1 Å), the target of the nucleophilic attack by water. Such a close contact with the carbonyl O atom is expected to draw the H1 atom away from its riding position on C1, making the C atom accessible to the nucleophile. In those chitinases that have Met in this position, an analogous interaction takes place between the C1—H1 group and the S atom. Thus, the role of Met or Gln is to prime the reaction intermediate for nucleophilic attack, but Gln218 in *Mm*Chi60 has an additional role: to maintain Asp151 in the 'up' position and to maintain Glu153 in the 'in' position relative to the active site (2.8 Å between Glu153 $O^{\varepsilon 2}$ and Gln218 $N^{\varepsilon 2}$; Fig. 5). This is the active conformation of the Asp151–Glu153 pair, with the closely interacting carboxyl groups likely to hold an H atom between them.

The first of the conserved triad of acidic residues, Asp149, remains constant in the centre of the β/α-barrel, underneath the active site. Its position in the three *Mm*Chi60 structures is similar to that in other known chitinases. The apparent role of this residue is to provide a negative potential to increase the pK_a of Asp151 nearby and, indirectly, of the catalytic Glu153.

Another interesting residue in the ligand-binding site is Asn221. Most studied chitinases have Asp in this position, with its proposed role being to increase the pK_a of the catalytic residue. Its mutation to Asn decreased the activity 20-fold in ChiB from *S. marcescens* (Synstad *et al.*, 2004). In *Mm*Chi60 Asn occurs naturally, which shows clearly that this enzyme has a different strategy to maintain an appropriately high pK_a of the catalytic Glu153. The presence of the pair Asn221 and the abovementioned Gln218 is not only observed in *Mm*Chi60. A corresponding pair of residues is found in chitinases from *L. lactis* (PDB entry 3ian), *B. cereus* (Hsieh *et al.*, 2010), *Streptomyces coelicolor* (New York SGX Research Center for Structural Genomics, unpublished work; PDB entry 3ebv) and *Aspergillus fumigatus* (Rush *et al.*, 2010) and in hevamine (Terwisscha van Scheltinga *et al.*, 1996). Interestingly, these chitinases from diverse organisms (bacteria, a fungus and a plant) have a common characteristic: a shallow substrate-binding groove (no insertions in the β/α-barrel). In contrast, other known chitinase structures have the above pair of residues replaced by Asp accompanied by Met, and most of those enzymes have 'tunnel-like' binding sites.

Structural comparisons allow us to discriminate the invariant elements of the enzymes from those which have been evolving. The constant features are probably the most essential to the catalytic activity or substrate recognition. The other elements probably indicate adaptation of different enzymes to their specific environments or point to alternative means to achieve some auxiliary functionality, such as fine-tuning the pK_a of the catalytic residue to be close to the ambient pH.

4.4. What is the basis of low-temperature optimization of the enzymatic activity?

It has been proposed that psychrophilic enzymes possess additional 'flexibility' which allows them to retain catalytic efficiency at low temperatures. It remains to be determined what one means by flexibility and to which parts of the protein it pertains. An examination of the *Mm*Chi60 structure indicates that a combination of factors are at play, including features of the active site together with other elements of the protein and even the overall topology of the enzyme. In the active site we observe flipping of the catalytic Glu153 coupled with rearrangement of the nearby loop 117–122. In the unliganded structure the loop is shifted 3 Å away from the active site in comparison with the protein–NAG_2 complex (see Supplementary movie[1]). The open conformation and the shallowness of the substrate-binding groove indicate the readiness of the enzyme to admit the substrate. On the other hand, the stable conformation of Asp151, which points towards the active site in all of the *Mm*Chi60 structures rather than into the interior of the protein, is conducive to catalysis. The substrate affinity of the binding groove can be supplemented by additional chitin-binding elements elsewhere in the protein: the chitin-binding domain and the pair of Trp residues

[1] Supplementary material has been deposited in the IUCr electronic archive (Reference: DW5036). Services for accessing this material are described at the back of the journal.

on the β/α-barrel. The distribution of substrate affinity over the 100 Å length of the protein would fully reveal its effectiveness towards long substrates. The long reach of the enzyme and its ability to cling to the surface of chitin could be a significant feature of its adaptation to the cold watery environment.

We thank Paweł Rodziewicz from the Laboratory of Proteomics and Metabolomics of IBCh PAN for performing mass spectrometry. The project was co-funded by the European Union within the European Regional Development Fund.

References

Aalten, D. M. F. van, Komander, D., Synstad, B., Gåseidnes, S., Peter, M. G. & Eijsink, V. G. (2001). *Proc. Natl Acad. Sci. USA*, **98**, 8979–8984.

Aalten, D. M. F. van, Synstad, B., Brurberg, M. B., Hough, E., Riise, B. W., Eijsink, V. G. & Wierenga, R. K. (2000). *Proc. Natl Acad. Sci. USA*, **97**, 5842–5847.

Afonine, P. V., Grosse-Kunstleve, R. W., Echols, N., Headd, J. J., Moriarty, N. W., Mustyakimov, M., Terwilliger, T. C., Urzhumtsev, A., Zwart, P. H. & Adams, P. D. (2012). *Acta Cryst.* D**68**, 352–367.

Aghajari, N., Van Petegem, F., Villeret, V., Chessa, J.-P., Gerday, C., Haser, R. & Van Beeumen, J. (2003). *Proteins*, **50**, 636–647.

Akagi, K., Watanabe, J., Hara, M., Kezuka, Y., Chikaishi, E., Yamaguchi, T., Akutsu, H., Nonaka, T., Watanabe, T. & Ikegami, T. (2006). *J. Biochem.* **139**, 483–493.

Altschul, S. F., Gish, W., Miller, W., Myers, E. W. & Lipman, D. J. (1990). *J. Mol. Biol.* **215**, 403–410.

Bendt, A., Hüller, H., Kammel, U., Helmke, E. & Schweder, T. (2001). *Extremophiles*, **5**, 119–126.

Boraston, A. B., Bolam, D. N., Gilbert, H. J. & Davies, G. J. (2004). *Biochem. J.* **382**, 769–781.

Bricogne, G., Vonrhein, C., Flensburg, C., Schiltz, M. & Paciorek, W. (2003). *Acta Cryst.* D**59**, 2023–2030.

Cowtan, K. (2000). *Acta Cryst.* D**56**, 1612–1621.

Cowtan, K. (2008). *Acta Cryst.* D**64**, 83–89.

Davies, G. J., Wilson, K. S. & Henrissat, B. (1997). *Biochem. J.* **321**, 557–559.

DeLano, W. L. (2002). *PyMOL*. http://www.pymol.org.

Emsley, P., Lohkamp, B., Scott, W. G. & Cowtan, K. (2010). *Acta Cryst.* D**66**, 486–501.

Fenice, M., Selbmann, L., Di Giambattista, R. & Federici, F. (1998). *Res. Microbiol.* **149**, 289–300.

Finn, R. D., Mistry, J., Tate, J., Coggill, P., Heger, A., Pollington, J. E., Gavin, O. L., Gunasekaran, P., Ceric, G., Forslund, K., Holm, L., Sonnhammer, E. L., Eddy, S. R. & Bateman, A. (2010). *Nucleic Acids Res.* **38**, D211–D222.

Gerday, C., Aittaleb, M., Arpigny, J. L., Baise, E., Chessa, J.-P., Garsoux, G., Petrescu, I. & Feller, G. (1997). *Biochim. Biophys. Acta*, **1342**, 119–131.

He, Y., Macauley, M. S., Stubbs, K. A., Vocadlo, D. J. & Davies, G. J. (2010). *J. Am. Chem. Soc.* **132**, 1807–1809.

Henrissat, B. & Bairoch, A. (1993). *Biochem. J.* **293**, 781–788.

Henrissat, B. & Davies, G. (1997). *Curr. Opin. Struct. Biol.* **7**, 637–644.

Hsieh, Y.-C., Wu, Y.-J., Chiang, T.-Y., Kuo, C.-Y., Shrestha, K. L., Chao, C.-F., Huang, Y.-C., Chuankhayan, P., Wu, W., Li, Y.-K. & Chen, C.-J. (2010). *J. Biol. Chem.* **285**, 31603–31615.

Huang, X. & Miller, W. (1991). *Adv. Appl. Math.* **12**, 337–357.

Kabsch, W. (2010). *Acta Cryst.* D**66**, 125–132.

Keyhani, N. O. & Roseman, S. (1999). *Biochim. Biophys. Acta*, **1473**, 108–122.

Lonhienne, T., Mavromatis, K., Vorgias, C. E., Buchon, L., Gerday, C. & Bouriotis, V. (2001). *J. Bacteriol.* **183**, 1773–1779.

Luo, Y., Zheng, Y., Jiang, Z., Ma, Y. & Wei, D. (2006). *Appl. Microbiol. Biotechnol.* **73**, 349–355.

McCoy, A. J., Grosse-Kunstleve, R. W., Adams, P. D., Winn, M. D., Storoni, L. C. & Read, R. J. (2007). *J. Appl. Cryst.* **40**, 658–674.

Morita, R. Y. & Haight, R. D. (1964). *Limnol. Oceanogr.* **9**, 103–106.

Murshudov, G. N., Skubák, P., Lebedev, A. A., Pannu, N. S., Steiner, R. A., Nicholls, R. A., Winn, M. D., Long, F. & Vagin, A. A. (2011). *Acta Cryst.* D**67**, 355–367.

Muzzarelli, R. A. (1977). *Chitin*. Oxford, New York: Pergamon Press.

Ohno, T., Armand, S., Hata, T., Nikaidou, N., Henrissat, B., Mitsutomi, M. & Watanabe, T. (1996). *J. Bacteriol.* **178**, 5065–5070.

Orikoshi, H., Baba, N., Nakayama, S., Kashu, H., Miyamoto, K., Yasuda, M., Inamori, Y. & Tsujibo, H. (2003). *J. Bacteriol.* **185**, 1153–1160.

Otwinowski, Z. & Minor, W. (1997). *Methods Enzymol.* **276**, 307–326.

Panjikar, S., Parthasarathy, V., Lamzin, V. S., Weiss, M. S. & Tucker, P. A. (2005). *Acta Cryst.* D**61**, 449–457.

Pannu, N. S. & Read, R. J. (2004). *Acta Cryst.* D**60**, 22–27.

Papanikolau, Y., Prag, G., Tavlas, G., Vorgias, C. E., Oppenheim, A. B. & Petratos, K. (2001). *Biochemistry*, **40**, 11338–11343.

Papanikolau, Y., Tavlas, G., Vorgias, C. E. & Petratos, K. (2003). *Acta Cryst.* D**59**, 400–403.

Payne, C. M., Baban, J., Horn, S. J., Backe, P. H., Arvai, A. S., Dalhus, B., Bjørås, M., Eijsink, V. G., Sørlie, M., Beckham, G. T. & Vaaje-Kolstad, G. (2012). *J. Biol. Chem.* **287**, 36322–36330.

Perrakis, A., Tews, I., Dauter, Z., Oppenheim, A. B., Chet, I., Wilson, K. S. & Vorgias, C. E. (1994). *Structure*, **2**, 1169–1180.

Rush, C. L., Schüttelkopf, A. W., Hurtado-Guerrero, R., Blair, D. E., Ibrahim, A. F., Desvergnes, S., Eggleston, I. M. & van Aalten, D. M. F. (2010). *Chem. Biol.* **17**, 1275–1281.

Sheldrick, G. M. (2008). *Acta Cryst.* A**64**, 112–122.

Shigemasa, Y. & Minami, S. (1996). *Biotechnol. Genet. Eng. Rev.* **13**, 383–420.

Stefanidi, E. & Vorgias, C. E. (2008). *Extremophiles*, **12**, 541–552.

Svitil, A. L. & Kirchman, D. L. (1998). *Microbiology*, **144**, 1299–1308.

Synstad, B., Gåseidnes, S., Van Aalten, D. M. F., Vriend, G., Nielsen, J. E. & Eijsink, V. G. (2004). *Eur. J. Biochem.* **271**, 253–262.

Terwilliger, T. C. (2003). *Acta Cryst.* D**59**, 38–44.

Terwisscha van Scheltinga, A. C., Hennig, M. & Dijkstra, B. W. (1996). *J. Mol. Biol.* **262**, 243–257.

Toratani, T., Kezuka, Y., Nonaka, T., Hiragi, Y. & Watanabe, T. (2006). *Biochem. Biophys. Res. Commun.* **348**, 814–818.

Vagin, A. & Teplyakov, A. (2010). *Acta Cryst.* D**66**, 22–25.

Van Petegem, F., Collins, T., Meuwis, M. A., Gerday, C., Feller, G. & Van Beeumen, J. (2003). *J. Biol. Chem.* **278**, 7531–7539.

Varrot, A., Schülein, M. & Davies, G. J. (2000). *J. Mol. Biol.* **297**, 819–828.

Violot, S., Aghajari, N., Czjzek, M., Feller, G., Sonan, G. K., Gouet, P., Gerday, C., Haser, R. & Receveur-Bréchot, V. (2005). *J. Mol. Biol.* **348**, 1211–1224.

Watanabe, T., Ito, Y., Yamada, T., Hashimoto, M., Sekine, S. & Tanaka, H. (1994). *J. Bacteriol.* **176**, 4465–4472.

Winn, M. D. *et al.* (2011). *Acta Cryst.* D**67**, 235–242.

Yaish, M. W., Doxey, A. C., McConkey, B. J., Moffatt, B. A. & Griffith, M. (2006). *Plant Physiol.* **141**, 1459–1472.

Zakariassen, H., Aam, B. B., Horn, S. J., Vårum, K. M., Sørlie, M. & Eijsink, V. G. (2009). *J. Biol. Chem.* **284**, 10610–10617.